β-Adrenergic control of sarcolemmal $Ca_V1.2$ abundance by small GTPase Rab proteins

Silvia G. del Villar[a], Taylor L. Voelker[a], Maartje Westhoff[a], Gopireddy R. Reddy[b], Heather C. Spooner[a], Manuel F. Navedo[b], Eamonn J. Dickson[a], and Rose E. Dixon[a,1]

[a]Department of Physiology and Membrane Biology, School of Medicine, University of California, Davis, CA 95616; and [b]Department of Pharmacology, School of Medicine, University of California, Davis, CA 95616

Edited by William A. Catterall, University of Washington, Seattle, WA, and approved January 11, 2021 (received for review August 24, 2020)

The number and activity of $Ca_V1.2$ channels in the cardiomyocyte sarcolemma tunes the magnitude of Ca^{2+}-induced Ca^{2+} release and myocardial contraction. β-Adrenergic receptor (*βAR*) activation stimulates sarcolemmal insertion of $Ca_V1.2$. This supplements the preexisting sarcolemmal $Ca_V1.2$ population, forming large "superclusters" wherein neighboring channels undergo enhanced cooperative-gating behavior, amplifying Ca^{2+} influx and myocardial contractility. Here, we determine this stimulated insertion is fueled by an internal reserve of early and recycling endosome-localized, presynthesized $Ca_V1.2$ channels. *βAR*-activation decreased $Ca_V1.2$/endosome colocalization in ventricular myocytes, as it triggered "emptying" of endosomal $Ca_V1.2$ cargo into the t-tubule sarcolemma. We examined the rapid dynamics of this stimulated insertion process with live-myocyte imaging of channel trafficking, and discovered that $Ca_V1.2$ are often inserted into the sarcolemma as preformed, multichannel clusters. Similarly, entire clusters were removed from the sarcolemma during endocytosis, while in other cases, a more incremental process suggested removal of individual channels. The amplitude of the stimulated insertion response was doubled by coexpression of constitutively active Rab4a, halved by coexpression of dominant-negative Rab11a, and abolished by coexpression of dominant-negative mutant Rab4a. In ventricular myocytes, *βAR*-stimulated recycling of $Ca_V1.2$ was diminished by both nocodazole and latrunculin-A, suggesting an essential role of the cytoskeleton in this process. Functionally, cytoskeletal disruptors prevented *βAR*-activated Ca^{2+} current augmentation. Moreover, *βAR*-regulation of $Ca_V1.2$ was abolished when recycling was halted by coapplication of nocodazole and latrunculin-A. These findings reveal that *βAR*-stimulation triggers an on-demand boost in sarcolemmal $Ca_V1.2$ abundance via targeted Rab4a- and Rab11a-dependent insertion of channels that is essential for *βAR*-regulation of cardiac $Ca_V1.2$.

L-type calcium channel | trafficking | β-adrenergic receptor | ion channel clustering | cardiac EC-coupling

The influx of Ca^{2+} through L-type Ca^{2+} channels ($Ca_V1.2$) is indispensable for cardiac excitation–contraction coupling (EC-coupling). These multimeric proteins consist of a pore-forming and voltage-sensing α_{1c} subunit, and auxiliary β- and $\alpha_2\delta$-subunits. In ventricular myocytes, $Ca_V1.2$ mainly localize to the t-tubule sarcolemma and open briefly, allowing a small amount of Ca^{2+} influx, in response to the wave of depolarization that travels through the conduction system of the heart from its point of origin, usually in the SA-node. This initial influx is amplified manifold though Ca^{2+}-induced Ca^{2+} release (CICR) from juxtaposed type 2 ryanodine receptors (RyR2) on the junctional sarcoplasmic reticulum, a short ∼12 nm across the dyadic cleft. The synchronous opening of thousands of RyR2 generates a transient, global elevation in intracellular calcium concentration ($[Ca^{2+}]_i$), resulting in contraction. Reducing $Ca_V1.2$ channel current (I_{Ca}) results in less CICR, smaller $[Ca^{2+}]_i$ transients, and less forceful contractions. Conversely, larger amplitude I_{Ca} elicits greater Ca^{2+} release from the sarcoplasmic reticulum, producing more forceful contractions. The level of Ca^{2+} influx through $Ca_V1.2$ channels therefore tunes EC-coupling.

I_{Ca} is a product of the number of channels in the sarcolemma and their open probability (P_o). Consequently, there are two possible, nonmutually exclusive strategies that may be adopted to alter I_{Ca} and consequently the magnitude of EC-coupling: 1) Adjust $Ca_V1.2$ channel activity (P_o) and 2) modify sarcolemmal $Ca_V1.2$ channel expression (N). The first strategy of increasing channel P_o has long been associated with β-adrenergic receptor (*βAR*)-mediated signaling in the heart (1–3). During acute physical or emotional stress, norepinephrine spills from sympathetic varicosities onto cardiomyocytes, activating *βAR*s. The ensuing $G_{\alpha s}$/adenylyl cyclase/cAMP/PKA signaling cascade culminates in PKA phosphorylation of several effector proteins, including $Ca_V1.2$ [or an element of their interactome (4)], enhancing their activity to generate this positive inotropic response.

As to the second strategy to increase I_{Ca}, there remains a paucity of information regarding the mechanisms regulating $Ca_V1.2$ channel abundance in the cardiomyocyte sarcolemma. Classic secretory transport literature suggests that $Ca_V1.2$ channels are trafficked from the endoplasmic reticulum to the *trans*-Golgi-network and onward to their dyadic position in the sarcolemma. Underscoring the importance of faithful $Ca_V1.2$ channel trafficking, altered $Ca_V1.2$ channel density has been reported in both failing (5) and aging (6) ventricular myocytes, and impaired anterograde trafficking of $Ca_V1.2$ channels to the t-tubules of human ventricular myocytes has been linked to dilated cardiomyopathy (7). Yet, despite the importance of tight homeostatic control of $Ca_V1.2$ channel trafficking to prevent Ca^{2+} dysregulation, the molecular steps defining $Ca_V1.2$ channel sorting and insertion remain poorly understood. Therefore, elucidation of the trafficking pathways that regulate $Ca_V1.2$ channel

Significance

The L-type voltage-gated Ca^{2+} channel $Ca_V1.2$ is essential for excitation–contraction coupling in the heart. During the fight-or-flight response, $Ca_V1.2$ channel activity is augmented as a result of PKA-mediated phosphorylation, downstream of β-adrenergic receptor activation. We discovered that enhanced sarcolemmal abundance of $Ca_V1.2$ channels, driven by stimulated insertion/recycling of specific $Ca_V1.2$-containing endosomes, is essential for β-adrenergic receptor-mediated regulation of these channels in the heart. These data reveal a conceptual framework of this critical and robust pathway for on-demand tuning of cardiac excitation–contraction coupling during fight-or-flight.

Author contributions: R.E.D. designed research; S.G.d.V., T.L.V., M.W., G.R.R., H.C.S., and R.E.D. performed research; S.G.d.V., T.L.V., M.W., G.R.R., and R.E.D. analyzed data; and S.G.d.V., M.F.N., E.J.D., and R.E.D. wrote the paper.

The authors declare no competing interest.

This article is a PNAS Direct Submission.

[1]To whom correspondence may be addressed. Email: redickson@ucdavis.edu.

This article contains supporting information online at https://www.pnas.org/lookup/suppl/doi:10.1073/pnas.2017937118/-/DCSupplemental.

Published February 8, 2021.

abundance is critical for our understanding of the pathophysiology of heart failure and myocardial aging, and could potentially reveal new therapeutic or rejuvenation targets. Along that vein, in the treatment of cystic fibrosis, multiple drugs are in various stages of use or development to improve trafficking to, or to amplify or stabilize, CFTR channels at the apical membrane of airway epithelial cells (8).

There exist no measurements of $Ca_V1.2$ channel lifetimes in cardiomyocytes, but pulse-chase experiments in immortalized cell lines support a lifetime of plasma membrane (PM)-localized $Ca_V1.2$ of ∼3 h (9), while total cellular $Ca_V1.2$ lifetime is >20 h (10). This disparity suggests membrane-$Ca_V1.2$ turns over much more dynamically than the total cellular channel content and implies ongoing local control by endosomal trafficking. Disturbance of the equilibrium between channel insertion/recycling and internalization would be predicted to lead to alterations in sarcolemmal $Ca_V1.2$ channel abundance. Trafficking of vesicular cargo through the endosomal pathway is regulated by Rab-GTPases, a >60-member family within the larger Ras superfamily of small GTPases (11, 12). Rab5 is involved in endocytosis and control of vesicular cargo influx into early endosomes (EEs; also called sorting endosomes), while Rab4 controls efflux of cargo out of EEs and fast recycling ($t_{1/2}$ ∼1 to 2 min) back to the PM (13). Rab11, expressed on recycling endosomes (RE; also called the endocytic recycling compartment or ERC), regulates slow recycling ($t_{1/2}$ ∼12 min) of cargo from this compartment back to the PM (13). In cortical neurons and pancreatic β-cells, activity-dependent $Ca_V1.2$ channel internalization has been postulated to play important roles in Ca^{2+} homeostasis, with implications for homeostatic synaptic plasticity and insulin production, respectively (11, 14). In mouse neonatal cardiomyocytes, Rab11b has been reported to limit $Ca_V1.2$ PM expression (15), while recent studies performed in HEK and HL-1 cells reported that endocytic recycling of cardiac $Ca_V1.2$ channels, regulates their surface abundance (10, 16). Despite this crucial information from other cell-types, there has been a lack of rigorous investigations, at the molecular level, into how $Ca_V1.2$ channel recycling is regulated in cardiac myocytes.

Here, we identify a dynamic, subsarcolemmal pool of $Ca_V1.2$-cargo–carrying endosomes that are rapidly mobilized to the ventricular myocyte sarcolemma along targeted Rab4a and Rab11a GTPase-regulated recycling pathways in response to *βAR*-stimulation. Using electrophysiology, cell biology, total internal reflection fluorescence (TIRF), and superresolution microscopy, we report that enhanced t-tubule sarcolemmal $Ca_V1.2$ abundance via targeted, isoproterenol (ISO)-stimulated recycling of these channels is essential for *βAR*-regulation of cardiac $Ca_V1.2$.

Results

Internal Pools of Presynthesized $Ca_V1.2$ Channels Reside on Endosomes. Recently, we reported that sarcolemmal $Ca_V1.2$ channel expression increases in the heart during *βAR* signaling (17). Activation of *βAR*s with ISO produced a rapid, PKA-dependent augmentation of $Ca_V1.2$ channel abundance along ventricular myocyte t-tubules. We hypothesized that an endosomal pool of $Ca_V1.2$ fuels the rapid, ISO-stimulated insertion of channels into the sarcolemma of ventricular myocytes (see *SI Appendix*, Fig. S1*A* for an overview of this model). To test this, we performed an examination of the distribution of $Ca_V1.2$ channels on EEs, REs, and late endosomes (LEs) in adult mouse ventricular myocytes (AMVMs) using two- or three-color Airyscan superresolution microscopy. Immunostained $Ca_V1.2$ channel cargo was observed on 15.1 ± 0.4% of early endosome antigen-1^+ ($EEA1^+$) pixels in male ventricular myocytes and on a similar 16.1 ± 0.7% in female myocytes ($P = 0.24$) (Fig. 1 *A* and *B*; see also *SI Appendix*, Fig. S2). Prefixation stimulation with 100 nM ISO led to a significant, 15 to 20% decrease in colocalization between $Ca_V1.2$ and EEA1 (male $P = 0.001$, female $P = 0.01$). We further narrowed our analysis to $Rab4^+$ EEs by performing triple-label experiments, costaining for $Ca_V1.2$, EEA1, and Rab4 (*SI Appendix*, Fig. S3). A similar trend was observed there such that 15.6 ± 1.3% of EEA1- and Rab4-coexpressing pixels were colocalized with $Ca_V1.2$, falling to 10.8 ± 0.6% in ISO-stimulated cells ($P = 0.008$). These data suggest that ISO activation of *βAR*s stimulates movement of $Ca_V1.2$ out of EEs and into another cellular compartment.

Cargo exiting the EE can be routed either to REs, LEs, or back to the sarcolemma via the fast-recycling pathway (*SI Appendix*, Fig. S1*A*) (12, 13). If *βAR* activation stimulates $Ca_V1.2$ channel trafficking from EEs into REs, then a testable prediction is that ISO should increase colocalization between $Ca_V1.2$ and Rab11 (a marker of REs). Accordingly, we examined the distribution of $Ca_V1.2$ on $Rab11^+$ REs, and found a population of $Ca_V1.2$-cargo-carrying REs, where $Ca_V1.2$ colocalized with 14.9 ± 0.5% of $Rab11^+$ pixels in males and with 13.3 ± 0.6% in females (Fig. 1 *C* and *D*). An 18% decrease in colocalization between $Ca_V1.2$ and Rab11 was observed in male cells treated with 100 nM ISO ($P = 0.002$). Data from female cardiomyocytes showed a similar downward trend in colocalization. These results do not support the hypothesis that $Ca_V1.2$ channels move from $Rab4^+$ EEs into REs in response to ISO. We next tested the hypothesis that ISO stimulation drives the trafficking of $Ca_V1.2$ channels from EEs to LEs; however, despite identifying a population of $Ca_V1.2$ channels on $Rab7^+$ LEs in male and female ventricular myocytes, ISO stimulation did not significantly alter the degree of Rab7/$Ca_V1.2$ colocalization (Fig. 1 *E* and *F*) ($P = 0.28$ in males, $P = 0.39$ in females). Having ruled out two of the three possibilities, we surmise that *βAR* stimulation drives an intracellular pool of $Ca_V1.2$ channels from $Rab4^+$ EEs into the fast-recycling pathway, and $Rab11^+$ REs into the slow recycling pathway.

ISO-Stimulated Enhancement of $Ca_V1.2$ Recycling Is Regulated by Rab4 and Rab11. Having determined that *βAR* stimulation decreases the number of $Ca_V1.2$ channels on EEs and REs, we next tested if Rab4-dependent fast-, and Rab11-dependent slow-recycling pathways facilitate enhancement of $Ca_V1.2$ delivery into the PM of transiently transfected tsA201 cells. While these cells do not recapitulate all of the intricacies of signaling in cardiomyocytes, we utilized them here because: 1) They provide a reductionist framework on which to test our Rab4 and Rab11 hypotheses in the absence of other voltage-gated channels; 2) they can be easily transfected, permitting manipulation of Rab-protein complement; and 3) they endogenously express *βAR*s (18). PM expression of $Ca_V1.2$ channels was monitored during activation of *βAR*s with 100 nM ISO. Clusters of channels were readily identified in the TIRF footprint of the cell (Fig. 2*A*). Upon wash-in of ISO, $Ca_V1.2$-tagRFP intensity in the TIRF footprint increased by an average of 1.37-fold over a period of minutes (Fig. 2*B*) ($\tau_{on} = 2.26 \pm 0.02$ min), in close agreement with previous results showing a 44.9 ± 6.2% increase in channels in ISO-stimulated AMVM sarcolemmas (17). An increased density (number/μm^2) of channel clusters in the TIRF footprint contributed to this elevation (Fig. 2*C*) ($P < 0.0001$). These results suggest that ISO stimulates enhanced recycling of $Ca_V1.2$ channels to the PM.

We tested the role of Rab4a in this dynamic response by coexpressing a mutant Rab4a with a single amino acid substitution (Q67L) that renders it resistant to GTP-hydrolysis, locking it in a GTP-bound, constitutively active state (CA-$Rab4a^{Q67L}$) (Fig. 2 *D*–*F*) (19). In these cells, addition of ISO stimulated a 1.69-fold increase in intensity, almost twice the maximal response observed in controls, and increased cluster density 2.4-fold (Fig. 2*F*) ($P = 0.002$). Interestingly, coexpression of CA-Rab4a had no effect on basal $Ca_V1.2$ cluster density before addition of ISO ($P = 0.08$) (Fig. 2 *C* and *F*) indicating that, even in this GTP-locked active state, ISO-stimulation is required to trigger the boost in $Ca_V1.2$ recycling. After ISO, the GTP-bound CA-Rab4a facilitates a larger, faster (1.76 ± 0.02 min) recycling response. This suggests that Rab4a plays a role in

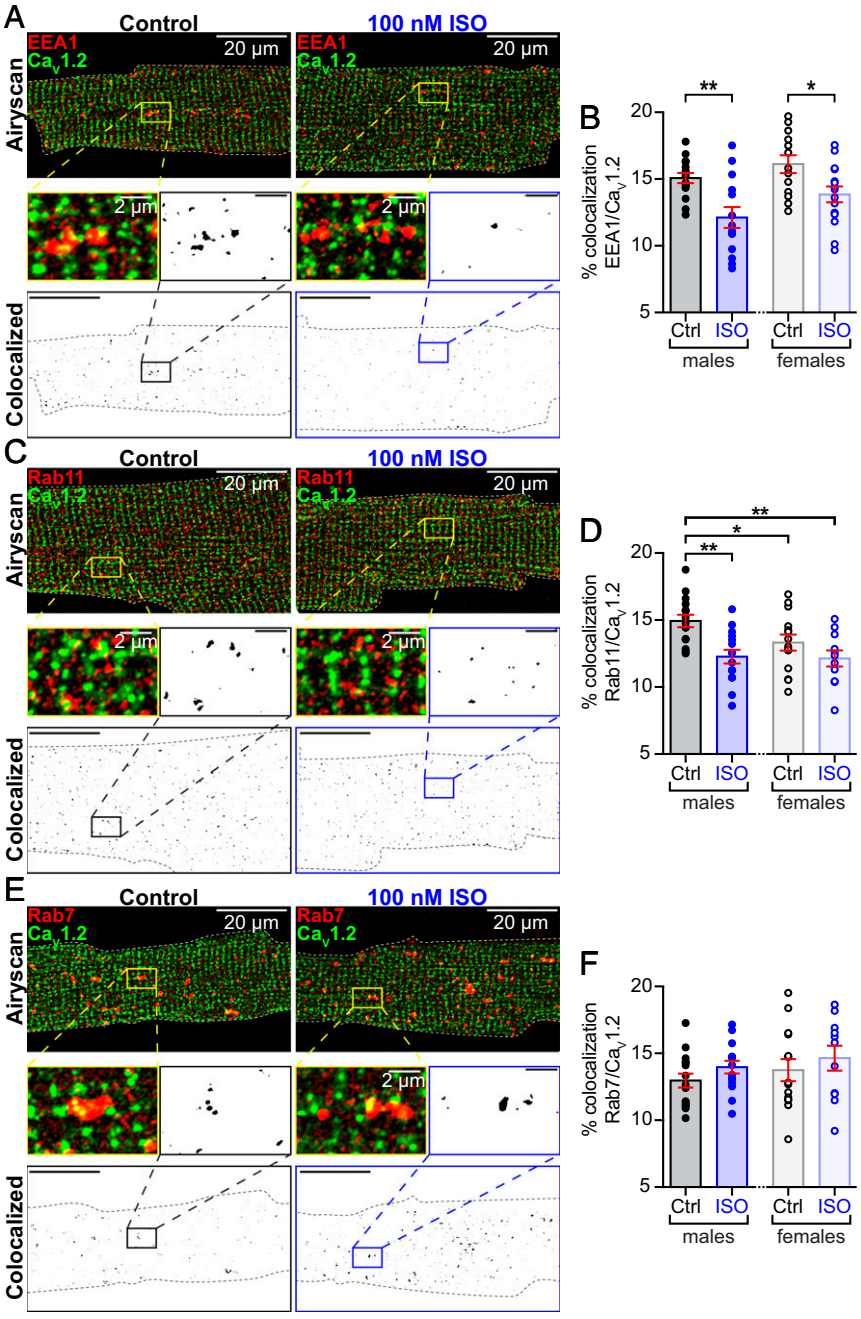

Fig. 1. Internal pools of presynthesized $Ca_V1.2$ channels reside on endosomes. (*A*) Two-color Airyscan superresolution images of control and 100 nM ISO-stimulated AMVMs immunostained to examine distributions of $Ca_V1.2$ and $EEA1^+$ early endosomes. Binary colocalization maps (*Bottom*) display pixels in which $Ca_V1.2$ and endosomal expression precisely overlapped. (*B*) Histograms showing percent colocalization between EEA1 and $Ca_V1.2$ in male and female AMVMs, in control (male: $n = 3$, $n = 15$; female $n = 3$, $n = 13$) and ISO-stimulated conditions (male: $n = 3$, $n = 14$; female $n = 3$, $n = 15$). (*C*) Immunostaining of $Ca_V1.2$ and $Rab11^+$ recycling endosomes and (*D*) accompanying histogram summarizing results from control (male: $n = 4$, $n = 15$; female $n = 3$, $n = 14$) and ISO conditions (male: $n = 3$, $n = 15$; female $n = 3$, $n = 11$). (*E*) Immunostaining of $Ca_V1.2$ and $Rab7^+$ LEs and lysosomes. (*F*) Histogram summarizing results from control (males: $n = 3$, $n = 15$, females: $n = 3$, $n = 14$) and ISO-stimulated AMVMs (males: $n = 3$, $n = 15$, females: $n = 3$, $n = 11$). Error bars indicate SEM. Two-way ANOVA $^{**}P < 0.01$; $^{*}P < 0.05$. Pictured are male AMVMs; for females see *SI Appendix*, Fig. S1.

βAR-stimulated channel recycling but also implies the involvement of an upstream effector.

To support this postulate, we examined the ISO response in cells expressing a dominant-negative, GDP-locked variant of Rab4 (DN-$Rab4^{S22N}$). Under these conditions, ISO-application failed to enhance $Ca_V1.2$ surface expression and instead a slight decrease in $Ca_V1.2$-tagRFP intensity and cluster density was observed in the PM over the course of the experiment (Fig. 2 *G–I*). These results confirm that Rab4a is part of the essential trafficking machinery that underlies the ISO-stimulated enhanced recycling of $Ca_V1.2$.

Since a subpopulation of $Ca_V1.2$ channels that localize to $Rab11^+$ REs was also identified in AMVMs (Fig. 1 *C* and *D*), we tested the role of Rab11a in this dynamic recycling response to ISO using a dominant-negative, GDP-locked DN-$Rab11a^{S25N}$. Despite impaired Rab11a function, an ISO-stimulated increase in $Ca_V1.2$-tagRFP intensity was still evident, albeit to a lesser extent than in controls (1.12-fold) (Fig. 2 *J* and *K*). This was accompanied by a 1.49-fold increase in cluster density ($P = 0.009$) (Fig. 2*L*). Accordingly, DN-Rab11a–mediated knock down of Rab11a activity generated ∼33% of the response seen in controls while knock down of Rab4a abolished the response (Fig. 2 *H* and *M*). These data suggest that upstream Rab4a activity is necessary, not only for fast recycling to the PM but also for transfer of $Ca_V1.2$ cargo from EEs to REs. Impaired Rab4a function creates a "road block" in the endosomal recycling system. The role of Rab4a in fast recycling was unmasked in cells with knocked down Rab11a activity, where τ_{on} of the stimulated recycling response was 0.96 ± 0.02 min (Fig. 2*K*), significantly faster than controls where both Rab4a and Rab11a were active (2.26 ± 0.02 min). A theoretical time course of the slow Rab11a-dependent contribution was calculated by subtracting the predominantly Rab4a-mediated recycling time-course in DN-Rab11a expressing cells from endogenous

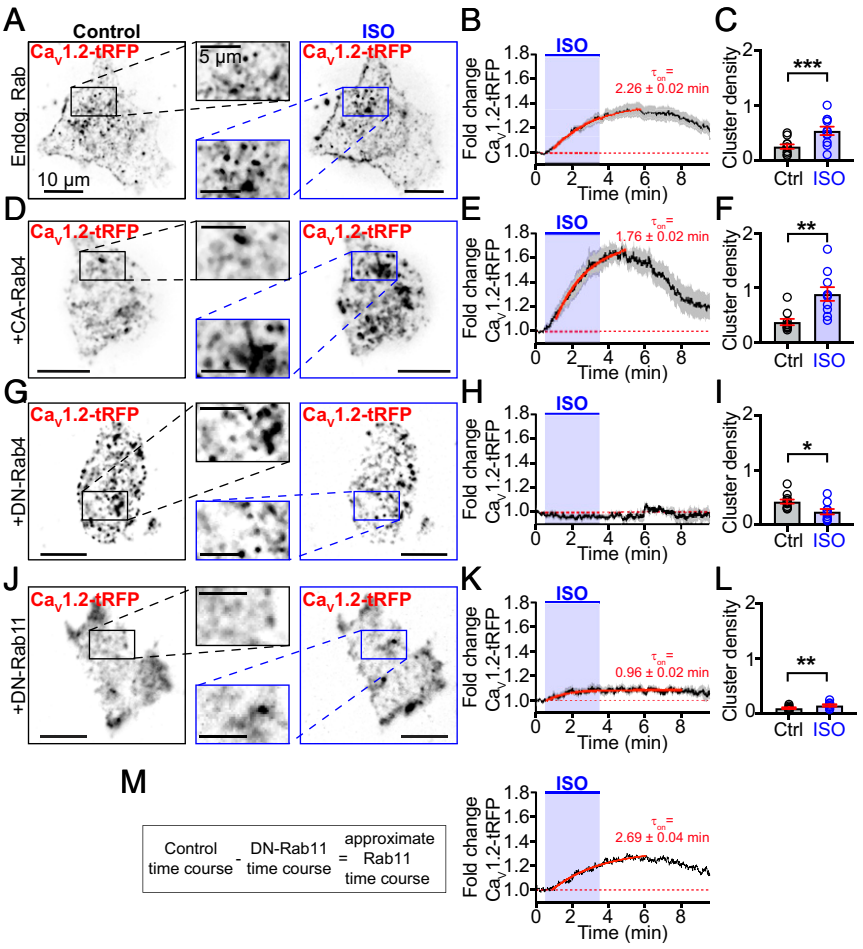

Fig. 2. Rab4a and Rab11a regulate an ISO-stimulated boost in $Ca_V1.2$ recycling. (*A*) TIRF images of $Ca_V1.2$-tRFP distribution in the PM of tsA-201 cells before (*Left*) and after 100 nM ISO (*Right*; $n = 18$). (*B*) Time course and kinetics (solid red line) of the fold-change in $Ca_V1.2$-tRFP intensity in the TIRF footprint before, during, and after ISO stimulation. (*C*) Histogram summarizing $Ca_V1.2$ channel cluster density (number/μm^2) in the TIRF footprint in control and ISO-stimulated conditions. (*D–F*) Same layout format in tsA-201 cells coexpressing constitutively active (GTP-locked) Rab4a ($n = 10$). (*G–I*) Same layout format in tsA-201 cells coexpressing dominant-negative (GDP-locked) Rab4a ($n = 12$). (*J–L*) Same layout format in tsA-201 cells coexpressing dominant-negative (GDP-locked) Rab11a ($n = 8$). (*M*) Calculation and resultant theoretical time-course and kinetics of Rab11a-dependent ISO-stimulated recycling. Data that passed a normality test (*C* and *L*) were analyzed with a paired *t* test, others (*F* and *I*) were analyzed with a nonparametric Wilcoxon test. ***$P < 0.001$; **$P < 0.01$; *$P < 0.05$.

Rab controls (Fig. 2*M*). This theoretical Rab11a-dependent response displayed a 1.29-fold increase in $Ca_V1.2$-tagRFP intensity and was well-fit with a single exponential function with a $\tau_{on} = 2.69 \pm 0.04$ min that was slower than control or Rab4a-mediated responses. Based on these data, our results suggest that $Ca_V1.2$ channels stimulated to recycle to the PM in response to *βAR* activation are sourced approximately one-third from the fast Rab4a, and two-thirds from the slow Rab11a recycling pathways.

Actin and Microtubule Disruption Impairs ISO-Stimulated $Ca_V1.2$ Recycling. We used Airyscan superresolution microscopy to examine $Ca_V1.2$ channel proximity to microtubules (MTs) and actin filaments (Fig. 3 *A* and *B*). Immunostaining with α-tubulin revealed the extensive MT cytoskeleton with its lattice, grid-like appearance in the subsarcolemma, transitioning to a more longitudinally oriented network deeper in the cell interior (Fig. 3*A*). $Ca_V1.2$ channels decorate the MTs in both locations. Phalloidin-staining of the actin network revealed the periodic alignment of sarcomeric actin (Fig. 3*B*). It is notoriously difficult to visualize cortical actin in cardiomyocytes due to the overwhelming abundance of sarcomeric actin but in many locations $Ca_V1.2$ channels were colocalized with actin (Fig. 3*B*, white arrowheads). The degree of colocalization between $Ca_V1.2$ and, in particular MTs, implies a role for the cytoskeleton in regulating channel availability.

To study the role of these cytoskeletal highways in *βAR*-stimulated $Ca_V1.2$ mobilization from endosomes, we examined EEA1-localized $Ca_V1.2$ channel populations in AMVMs treated with cytoskeletal disruptors. Accordingly, freshly isolated myocytes were treated for 2 h with 10 μM nocodazole, a drug known to prevent addition of tubulin to dynamic MTs, and depolymerize the stable variety (20). Immunostaining with anti–α-tubulin confirmed the treatment had substantially disordered the MTs (Fig. 3*C* and *SI Appendix*, Fig. S4 *A* and *B*). In this and upcoming experimental series, we refer to cells that did not receive cytoskeletal disruptors as "untreated." As in untreated cells (Fig. 1 *A* and *B*), $Ca_V1.2$ was observed to colocalize with a subpopulation of EEs ($16.9 \pm 0.6\%$) (Fig. 3 *D* and *E*). However, in cells stimulated with 100 nM ISO prior to fixation, the reduction in colocalization between EEA1 and $Ca_V1.2$ we had previously observed in untreated cells was absent in nocodazole-treated cells, instead remaining at $17.5 \pm 0.7\%$ ($P = 0.51$ compared to nocodazole-treated control). These data suggest that MT network disruption prevents the "emptying" of $Ca_V1.2$ channel cargo from the EEs into the sarcolemma and support a role for MTs and their associated motor proteins as conduits for ISO-stimulated $Ca_V1.2$ recycling.

We then examined the role of the actin cytoskeleton by disrupting it with latrunculin A (lat-A; 5 μM for 2 h), which facilitates F-actin depolymerization and prevents polymerization by sequestering actin monomers (20). Alexa Fluor 647-conjugated phalloidin staining of filamentous-actin (F-actin) was used to visually confirm lat-A–mediated actin disruption (Fig. 3*F* and *SI Appendix*, Fig. S4 *C–E*). In lat-A–treated myocytes, $Ca_V1.2$ and EEA1 colocalization was similar to untreated controls ($16.2 \pm 0.7\%$ versus $15.1 \pm 0.4\%$; $P = 0.14$). However, ISO-stimulation did not affect colocalization levels ($16.7 \pm 0.5\%$; $P = 0.64$) (Fig. 3 *G* and *H*). In addition, in cells cotreated with nocodazole and lat-A, ISO-stimulation actually promoted a small, but significant increase in colocalization between $Ca_V1.2$ and EEA1 ($P = 0.03$) (Fig. 3 *I* and *J*). These data indicate a profound alteration in the endosomal pathway where recycling and or endocytosis have

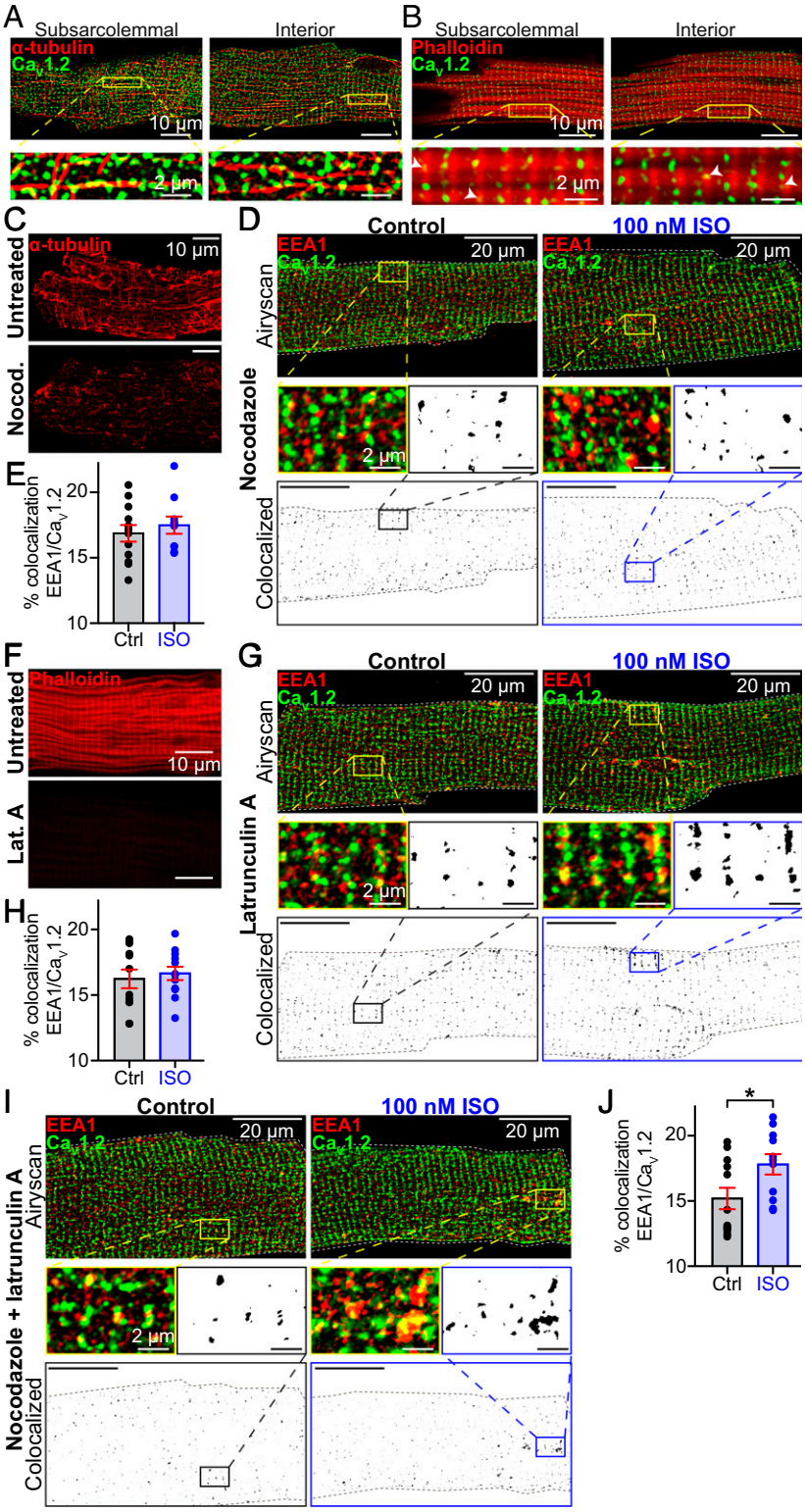

Fig. 3. Actin and MT polymerization are essential for ISO-stimulated $Ca_V1.2$ recycling. Two-color Airyscan images of fixed AMVMs immunostained to examine the relative localization of $Ca_V1.2$ and (*A*) α-tubulin, or (*B*) phalloidin-stained actin. (*C*) The distribution of α-tubulin in untreated (*Top*) and nocodazole-treated AMVMs (*Bottom*). (*D*) Airyscan images of $Ca_V1.2$ and EEA1 distribution in nocodazole-treated control ($n = 3$, $n = 12$; *Left*) and ISO-stimulated ($n = 3$, $n = 10$; *Right*) AMVMs. (*Bottom*) Binary colocalization maps display pixels in which $Ca_V1.2$ and EEA1 expression precisely overlapped. (*E*) Histogram summarizing percent colocalization of EEA1 with $Ca_V1.2$ in nocodazole-treated cells. (*F*) Actin distribution in untreated (*Top*) and lat-A–treated cells (*Bottom*). (*G*) Airyscan images and binary colocalization maps of $Ca_V1.2$ and EEA1 distribution in lat-A–treated control ($n = 3$, $n = 12$; *Left*) and ISO-stimulated ($n = 3$, $n = 12$; *Right*) AMVMs. (*H*) Histogram showing percent colocalization of EEA1 with $Ca_V1.2$ in lat-A–treated AMVMs. (*I*) Airyscan images and binary colocalization maps of AMVMs treated with both lat-A and nocodazole under control ($n = 3$, $n = 12$) and ISO stimulated conditions ($n = 3$, $n = 11$), with accompanying summary histogram (*J*). Statistical analyses were unpaired *t* tests. $^*P < 0.05$.

been impaired, creating an "endosomal traffic jam," leading to accumulation of cargo on the endosomes, with no cytoskeletal highways to transport the cargo to its destination.

Cytoskeletal Disruption Alters ISO-Stimulated $Ca_V1.2$ Dynamics and Recycling. Real-time visualization and quantification of the effects of cytoskeletal disruption on channel trafficking was performed using transduced AMVMs isolated from mice that had received a retro-orbital injection of AAV9-$Ca_V\beta_{2a}$-paGFP. This auxiliary subunit of $Ca_V1.2$ binds to the pore-forming subunit with a 1:1 stoichiometry and acts in this context as a biosensor, reporting the location of the subset of $Ca_V1.2$ α_{1c} it interacts with. This approach was previously validated by our group (17), with superresolution microscopy experiments confirming that $Ca_V\beta_{2a}$-paGFP and α_{1c} colocalize, and unlike overexpression of α_{1c}, at these concentrations we have found that $Ca_V\beta_{2a}$-paGFP

transduction does not appreciably affect $Ca_V1.2$ α_{1c} expression as indicated by unaltered basal channel cluster sizes. Additional validation performed for this study revealed the level of $Ca_V\beta_{2a}$-paGFP expression we achieve does not alter I_{Ca} inactivation kinetics or PKA modulation of the channels (Table 1 and *SI Appendix*, Fig. S5), as has been reported in previous studies with more robust overexpression (21, 22). Finally, since $Ca_V\beta_{2a}$ can localize to the membrane independently of α_{1c} (9, 21) we performed a final validation by comparing the time course of ISO-stimulated augmentation of $Ca_V\beta_{2a}$-paGFP expression in the TIRF footprint with that of I_{Ca} modulation. We fiound that the time course of the ISO-stimulated up-regulation in current density coincides with the $Ca_V\beta_{2a}$-paGFP–indicated increase in channel expression (*SI Appendix*, Fig. S5 *G–J*), supporting the use of $Ca_V\beta_{2a}$-paGFP as a proxy for α_{1c}.

We examined the dynamic channel trafficking response to ISO in untreated AMVMs (i.e., in the absence of cytoskeletal disruptors) using TIRF microscopy. Discrete puncta of $Ca_V\beta_{2a}$-paGFP decorated the TIRF footprint of the myocyte during control frames and additional puncta/clusters were seen to appear in the TIRF footprint supplementing the initial complement after perfusion with 100 nM ISO (Fig. 4*A* and Movie S1). Given our endosome/$Ca_V1.2$ immunostaining results (Fig. 1), this may represent endosomal cargo mobilized in response to ISO from subsarcolemmal locations deeper within the cell. In agreement with this, Three-dimensional (3D)-plots of $Ca_V\beta_{2a}$-paGFP intensity over time and cell depth, constructed from four-dimensional (4D)-spinning disk confocal experiments performed on transduced AMVMs at 37 °C, indicated $Ca_V\beta_{2a}$-paGFP was mobilized from several microns within the cell, and moved toward the surface in response to ISO (*SI Appendix*, Fig. S6). At physiological temperature, the response to ISO proceeded monoexponentially with a $\tau = 4.12$ s until $Ca_V\beta_{2a}$-paGFP intensity reached a plateau (*SI Appendix*, Fig. S6 *C–E*), presumably achieved when the endosomal pool of channels had been depleted and balance between insertion and endocytosis reached a new equilibrium.

To test the hypotheses that ISO treatment increases sarcolemmal expression of $Ca_V1.2$ by stimulating channel insertion/recycling, and that cytoskeletal highways carry these recycling channels to their destination, we performed "image math" (*Materials and Methods*) on TIRF time series to quantify the subpopulations of $Ca_V\beta_{2a}$-paGFP in the TIRF-footprint that were 1) inserted, 2) endocytosed, and 3) stably expressed during ISO stimulation. Responses to ISO in untreated AMVMs were compared to those in cells treated with nocodazole, lat-A, or a combination of both (Fig. 4). Live-cell time series experiments revealed a dynamic population of $Ca_V\beta_{2a}$-paGFP in all cells examined (Movies 1–4), although the dynamics were appreciably less in cells that received cytoskeletal disrupting treatments, supporting the idea that both F-actin and MTs are important conduits of this response. The number of channels at the sarcolemma at any given time, is dictated by the balance between channel insertions via the biosynthetic delivery and endosomal recycling pathways, and channel removals via endocytosis. In untreated cells, ISO stimulation heavily shifted the balance in favor of insertion, implying a stimulated insertion/recycling process (Fig. 4 *A* and *E–G*). This mismatch between insertion and endocytosis produced a $27.95 \pm 4.31\%$ increase in sarcolemmal $Ca_V\beta_{2a}$-paGFP expression (Fig. 4*E*). The time course of ISO-stimulated insertions of channels in untreated AMVMs can be observed in the regions-of-interest (ROIs) highlighted in Fig. 4*A*. Examination of these time courses revealed rapid step-like insertion profiles, suggesting that $Ca_V1.2$ appear to often insert into the sarcolemma as preformed clusters, containing many channels (Fig. 4 *A*, *i–iii*, Fig. 4 *B*, *ii* and *iii*, Fig. 4 *C*, *ii* and *iii*, and Fig. 4 *D*, *i* and *ii*). In some cases, a delivery hub was evident, where a succession of channel clusters appeared to insert one after the other (Fig. 4 *A*, *ii* and Fig. 4 *B*, *iii*). Channel endocytosis also appeared to involve removal of channel clusters in some instances (Fig. 4 *C*, *i* and Fig. 4 *D*, *iii*), while in other ROIs, a slower, gradual removal of potentially individual channels was more evident (Fig. 4 *B*, *i*).

Recycling of endosomal cargo back to the PM is known to rely on both MTs and actin (23). Indeed, cytoskeletal disruption reduced the magnitude of the ISO-stimulated augmentation of sarcolemmal $Ca_V\beta_{2a}$-paGFP expression compared to untreated cells (Fig. 4*E*). How the two elements of the cytoskeleton affected the ISO-stimulated change in sarcolemmal expression varied somewhat, as revealed by examination of insertion and endocytosis events in each AMVM cohort. Anterograde transport and targeting of $Ca_V1.2$ to the t-tubule membrane is known to occur along MTs, anchored there via the BAR-domain–containing protein, BIN1 (also known as amphiphysin II) (24). Here, our experiments were focused not on long-distance trafficking from the *trans*-Golgi to the membrane, but rather from the local endosome pool of channels and thus channel dynamics were observed over short 3-min periods before and after application of ISO. Our data indicate that nocodazole-mediated MT disruption reduced ISO-stimulated insertion of $Ca_V\beta_{2a}$-paGFP by an average of ~70% compared to untreated cells (Fig. 4*F*). Channel internalization and the lifetime of channels in the membrane was not affected by the degree of MT disruption tested here, as both endocytosed and static channel population sizes were not significantly altered by this treatment (Fig. 4 *G* and *H*).

Actin disruption with lat-A in contrast had no significant effect on channel insertion compared to untreated cells (Fig. 4*F*). In neurons and HEK293 cells, interactions between $Ca_V1.2$ and the actin-interacting protein α-actinin have been found to stabilize $Ca_V1.2$ channel expression at the PM (25, 26). A notable trend toward increased endocytosis of $Ca_V\beta_{2a}$-paGFP in lat-A–treated cells was detected but this failed to reach significance assessed by a one-way ANOVA test (Fig. 4*G*). There was also a trending increase in the fraction of stable $Ca_V\beta_{2a}$-paGFP in the TIRF footprint that appeared to be left "stranded" there (Fig. 4*H*), perhaps reflective of incomplete internalization of $Ca_V\beta_{2a}$-paGFP due to the lack of actin dynamics and the disrupted cortical actin network. This effect was not statistically different from controls but was significantly different from nocodazole-treated cells. Finally, combined treatment with nocodazole and lat-A actually reduced the overall expression of $Ca_V\beta_{2a}$-paGFP in the TIRF footprint by $8.63 \pm 6.76\%$ over the course of the experiment (Fig. 4 *F* and *G*). This occurred when the balance of endocytosis and insertion/recycling shifted in favor of endocytosis. Collectively, these data suggest that MTs and actin are both important conduits of *βAR*-stimulated $Ca_V1.2$ recycling, with MTs playing the major role in channel insertion.

βAR Mediated I_{Ca} Regulation Is Abrogated by Cytoskeletal Disruption. To ascertain whether ISO-stimulated recycling of $Ca_V1.2$ channels into the cardiomyocyte sarcolemma makes any functional contribution to the *βAR* regulation of these channels, we performed whole-cell patch-clamp recordings on freshly isolated AMVMs under various cytoskeleton disrupting conditions. Stimulation of untreated cardiomyocytes with 100 nM ISO, produced a 1.65 ± 0.19-fold enhancement of I_{Ca} (Fig. 5 *A* and *B*) and caused a 13.33 ± 1.49-mV leftward-shift in the voltage-dependence of conductance (measured as the difference between $V_{1/2}$ of each fit; $P < 0.0001$) (Fig. 5*C* and Table 1). In addition, we observed an increase in the slope steepness of the Boltzmann function used to fit the G/G_{max} data from 5.45 ± 0.84 in controls to 4.90 ± 1.06 in 100 nM ISO (Fig. 5*C* and Table 1), suggesting a potential increase in cooperative gating behavior (17).

The impact of MT disruption on the I_{Ca} response to ISO was tested in AMVMs incubated with nocodazole. This dose and duration of treatment did not alter control I_{Ca} amplitude (compared to untreated control). Indeed, none of the cytoskeletal disrupting treatments had any significant effect on control I_{Ca} with all of them peaking between −3.78 and −4.07 pA/pF (Fig. 5 *B*, *E*, *H*, and *K*).

Table 1. ISO-stimulated changes in peak I_{Ca} and voltage dependence of G/G_{max}

		$V_{1/2}$ (mV)		Slope factor	
	Fold-change in peak I_{Ca}	Control	ISO	Control	ISO
Untreated	1.67 ± 0.19	−7.57 ± 0.95	−20.90 ± 1.14***	5.45 ± 0.84	4.90 ± 1.06
Nocodazole	1.18 ± 0.08*	−9.27 ± 0.42	−15.97 ± 0.83***	5.00 ± 0.39	5.24 ± 0.71
Latrunculin A	1.39 ± 0.13	−13.03 ± 0.87	−18.95 ± 0.97***	5.51 ± 0.76	5.33 ± 0.88
Noco + Lat.A	1.01 ± 0.11**	−12.63 ± 1.40	−15.16 ± 1.53	7.32 ± 1.24	7.82 ± 1.36
$Ca_V\beta_{2a}$-paGFP	2.01 ± 0.12	4.10 ± 1.10	−9.55 ± 0.95***	10.27 ± 0.97	5.70 ± 0.86*

Mean ± SEM values obtained for the fold-change peak I_{Ca} (one-way ANOVA with Dunnett's multiple comparisons test; * indicates significant difference from the fold-change in untreated AMVMs), and for the $V_{1/2}$ and slope factor of the voltage dependence of G/G_{max} fits (one-way ANOVA). ***$P < 0.001$; **$P < 0.01$; *$P < 0.05$.

However, nocodazole blunted the I_{Ca} response to ISO by ∼72% (1.18 ± 0.08-fold increase versus 1.65-fold change in untreated cells), halved the magnitude of leftward-shift of the voltage dependence of conductance (6.73 ± 1.38-mV versus the 13.33-mV shift in untreated cells), and eliminated the tendency toward cooperativity indicated by the slope of the Boltzmann function used to fit the G/G_{max} (Fig. 5 *D–F* and Table 1).

We used the same experimental paradigm to test whether the actin cytoskeleton plays any role in the functional regulation of $Ca_V1.2$ by *βAR*s. Cells treated with lat-A exhibited a 40% reduction in the I_{Ca} augmentation response to ISO compared to controls (Fig. 5 *G* and *H* and Table 1), and a similar halving of the leftward-shift in the voltage-dependence of conductance as in nocodazole-treated cells (5.92 ± 1.63 shift) (Fig. 5*I* and Table 1). ISO stimulation produced G/G_{max} data that was well fit with a Boltzmann function that was less steep than in ISO-stimulated untreated cells but still indicated enhanced cooperativity (Fig. 5*I* and Table 1).

Finally, we examined the effect of ISO on I_{Ca} when both MTs and actin filaments were disrupted with a combined nocodazole and lat-A treatment. Under these conditions, *βAR*-mediated regulation of $Ca_V1.2$ was essentially abolished (Fig. 5 *J* and *K*), with ISO, generating only a 1.01 ± 0.11-fold increase in I_{Ca}, representing a 98% reduction in the response compared to untreated cells. The leftward-shift in the voltage-dependence of conductance was reduced to 2.54 ± 1.49 mV, equivalent to only 20% of the response seen in untreated cells. The slope factor of the Boltzmann-function used to fit the data were less steep than untreated cells in both control and ISO-stimulated conditions, indicating reduced cooperativity. These functional data collectively indicate that an intact cytoskeleton is an essential requirement for *βAR*-mediated regulation of $Ca_V1.2$.

Clustering of $Ca_V1.2$ Channels Is Supported by the Cytoskeleton. The observation that channel cooperativity was altered in AMVMs with disrupted cytoskeletal elements implies that the cytoskeleton might be important not only for *βAR*-mediated regulation of $Ca_V1.2$ but also for the stabilization and support of channel clusters. We tested this idea by examining $Ca_V1.2$ channel distribution in AMVMs using ground-state depletion (GSD) superresolution nanoscopy. Furthermore, since PKA is known to stimulate I_{Ca} more robustly at the t-tubules compared to the crest due to better coupling between *βAR*s and the channels located there (27, 28), we investigated whether ISO-stimulated insertions occurred preferentially in the t-tubules by examining and comparing the $Ca_V1.2$ populations in the t-tubule and crest regions of the sarcolemma. ISO-stimulation resulted in the formation of $Ca_V1.2$ channel superclusters in AMVMs, which in the t-tubules were on average 22.5% larger (Fig. 6 *A* and *E*), and in the crest, 25.7% larger than the clusters in control AMVMs (*SI Appendix*, Fig. S7 *A* and *B*). Superclustering could occur due to small clusters fusing together to form larger ones, or alternatively, could reflect enhanced sarcolemmal expression of $Ca_V1.2$. If the superclusters form because of enhanced insertion/exocytosis of $Ca_V1.2$ into the sarcolemma, then a testable prediction is that the intensity of the fluorescence emission (normalized to the cell area) should be increased. In contrast, if the superclusters simply reflect fusion of existing sarcolemmal $Ca_V1.2$ clusters then the total fluorescence intensity should be similar in control and ISO-treated cells. Accordingly, in the t-tubules, normalized total integrated density was significantly larger in ISO-treated cells than controls (Fig. 6*F*) ($P < 0.001$), in agreement with the idea that *βAR*-activation stimulates enhanced sarcolemmal insertion and resultant superclustering of $Ca_V1.2$ channels. Interestingly, in the sarcolemmal crest, total integrated density was unaltered by ISO, suggesting small clusters there may have fused together to form larger clusters (*SI Appendix*, Fig. S7*D*). This was supported by a rightward shift of the cumulative frequency distribution of crest channel cluster areas after ISO (*SI Appendix*, Fig. S7*G*). Based on these observations, the t-tubule sarcolemma appears to be the main site of ISO-stimulated $Ca_V1.2$ insertions.

Cytoskeletal disruption with nocodazole (Fig. 6*B*), lat-A (Fig. 6*C*), or a combination of the two (Fig. 6*D*), did not affect basal channel expression in the t-tubules, as indicated by similar cluster areas and total integrated density values (Fig. 6 *E* and *F*). These results validate the unaltered I_{Ca} observed in unstimulated cells from each of our four experimental groups (Fig. 5) and supports the postulate that the lifetime of these channels in the membrane is longer than the 2-h cytoskeletal disruption period. In addition, ISO-stimulation failed to induce superclustering or enhanced t-tubule membrane expression of $Ca_V1.2$ in AMVMs (Fig. 6 *E* and *F*). Altogether, these data suggest that both intact MTs and actin are necessary for the formation of $Ca_V1.2$ super clusters in response to ISO stimulation.

Discussion

The data presented in the present study provide a report of an endosomal pool of $Ca_V1.2$ channels in cardiomyocytes that undergoes rapid, targeted mobilization to the t-tubule sarcolemma in response to *βAR*-activation, effectively creating an "on-demand" trafficking pathway to facilitate a positive inotropic response during fight-or-flight. We present six major findings: 1) Intracellular pools of $Ca_V1.2$ channels are present on EEs, REs, and in LEs and lysosomes in AMVMs; 2) *βAR*-activation triggers $Ca_V1.2$ mobilization from EEs and REs to the sarcolemma via Rab4a-dependent fast, and Rab11a-dependent slow recycling pathways; 3) $Ca_V1.2$ are often inserted or removed from the sarcolemma as large multichannel clusters, rather than individual channels; 4) stimulated insertion of $Ca_V1.2$ channels occurs along MTs; 5) the endosomal pool of $Ca_V1.2$ is fueled by actin-dependent endocytosis; and finally, 6) adrenergic regulation of $Ca_V1.2$ is abrogated by cytoskeletal disruption and loss of this dynamic recycling response. On the basis of these data, we present a working model (*SI Appendix*, Fig. S1) for *βAR*-regulation of cardiac $Ca_V1.2$ channels in which stimulated recycling of $Ca_V1.2$, from subsarcolemmal pools of $Rab4a^+$ and $Rab11a^+$ endosomes, results in enhanced

PHYSIOLOGY

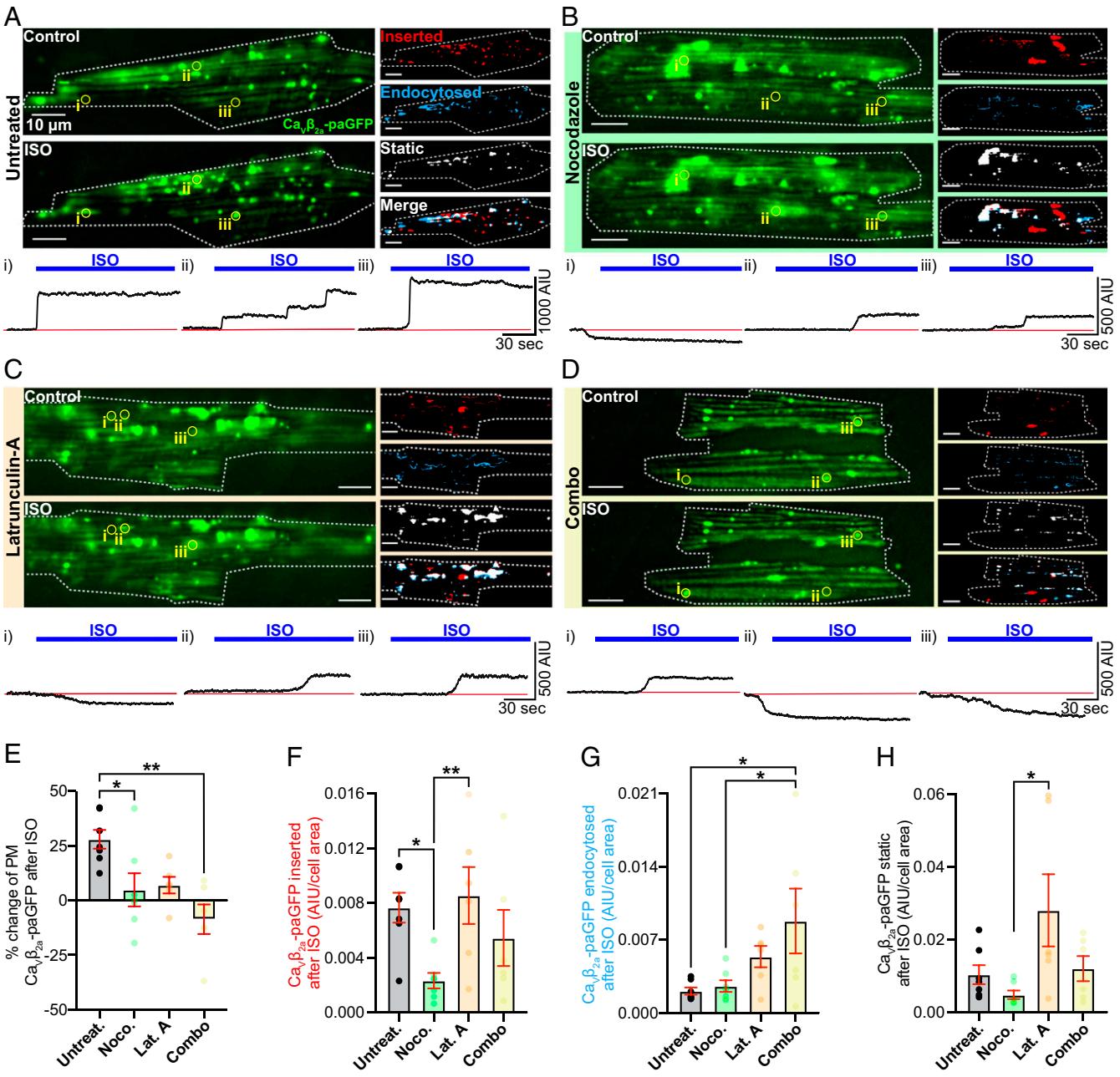

Fig. 4. Dynamic imaging to unmask the mobile channel population. (*A*) TIRF images of GFP fluorescence emission from $Ca_V\beta_{2a}$-paGFP transduced AMVMs before (*Top*) and after 100 nM ISO (*Bottom*). Images illustrating inserted, endocytosed, static, and merged channel populations are shown to the right. (*Bottom*) Time course of the changes in $Ca_V\beta_{2a}$-paGFP intensity in ROIs (*i–iii*) indicated by yellow circles on TIRF images ($n = 5$, $n = 7$). Same format for cells pretreated with (*B*) nocodazole ($n = 5$, $n = 7$), (*C*) lat-A ($n = 3$, $n = 6$), or (*D*) both cytoskeleton disruptors ($n = 3$, $n = 6$). (*E–H*) Histograms summarizing statistics for these experiments analyzed with Kruskal–Wallis tests. $^{**}P < 0.01$; $^{*}P < 0.05$.

expression of $Ca_V1.2$ at the t-tubule membrane of AMVMs. Resultant superclustering and cooperative gating of $Ca_V1.2$ channels contributes to the enhanced I_{Ca} and inotropic response.

Our data revealed pools of intracellular $Ca_V1.2$ channels on EEA1 and $Rab4^+$ EEs, on $Rab11^+$ REs, and in $Rab7^+$ LEs and lysosomes. In response to ISO, EE- and RE-localized channels underwent rapid recycling into the sarcolemma via the Rab4a-dependent fast-recycling pathway and the slower, Rab11a recycling pathway. While this report of stimulated recycling of a recruitable intracellular reservoir of $Ca_V1.2$ in cardiomyocytes is unique, small GTPase choreographed-recycling of endosome-localized ion channel pools are well-known to play a role in fine-tuning cellular responses to various stimuli including *βAR* stimulation. For example, in neurons, intracellular AMPA receptors (AMPAR) located on REs undergo Rab11-dependent recycling to the PM of dendritic spines in response to PKA-mediated phosphorylation of their GluA1 subunit at S845 downstream of β_2AR stimulation (reviewed in ref. 29). In the collecting ducts of the kidney, vasopressin release initiates a G_s-coupled signaling cascade that triggers PKA-mediated phosphorylation of aquaporin-2 (AQP2) at S256 and consequent recycling of AQP2 from $Rab11^+$ REs to the apical PM (30, 31). In the heart, acute stress initiates Rab11-dependent mobilization of endosomal reservoirs of SUR2-containing K_{ATP} channels and of KCNQ1-containing

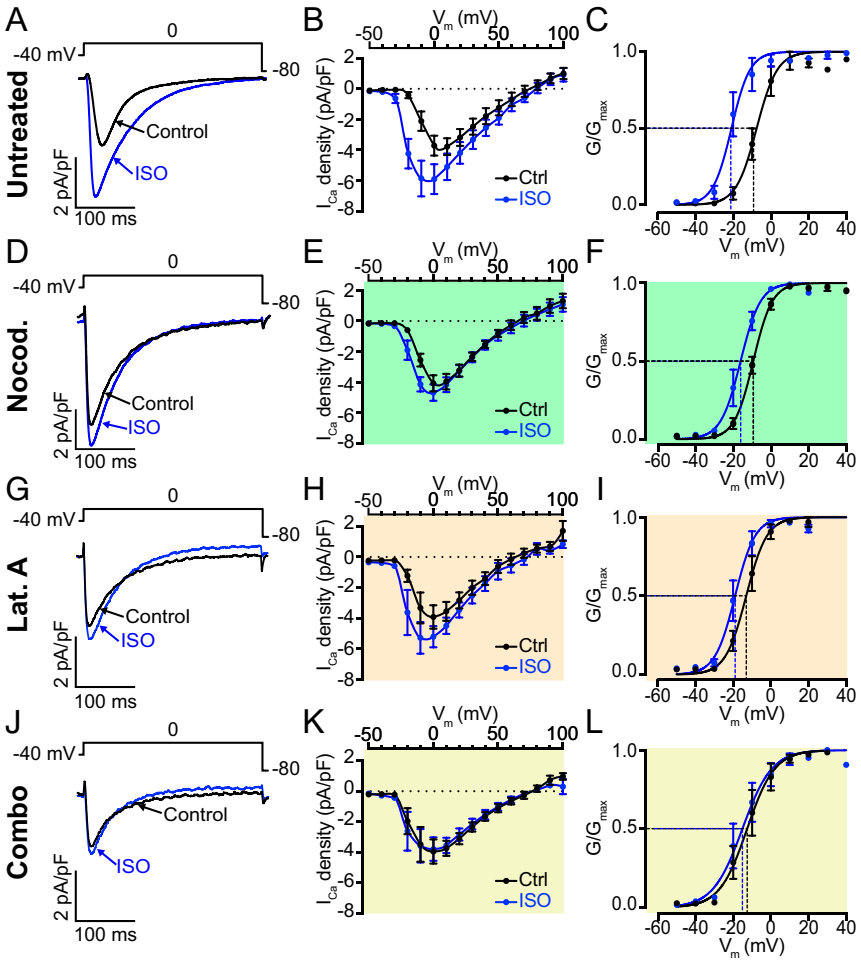

Fig. 5. βAR-mediated I_{Ca} enhancement is blunted by reducing dynamic channel insertion. (*A*) Whole-cell currents elicited from a representative AMVM during a 300-ms depolarization step from −40 mV to 0 mV before (control: black) and during application of 100 nM ISO (blue). (*B*) I-V plot summarizing the results from $n = 7$ cells (from $n = 7$ animals) subjected to test potentials ranging from −50 mV to +100 mV. Currents were normalized to cell capacitance to generate current density. (*C*) Voltage-dependence of the normalized conductance (G/G_{max}) before and during ISO application, fit with Boltzmann functions. (*D–F*) Whole-cell currents (*D*), I-V (*E*), and G/G_{max} plots (*F*) from AMVMs pretreated for 2 h with 10 μM nocodazole ($n = 4$, $n = 7$). (*G*, *H*) The same for cells treated with 5 μM lat-A ($n = 5$, $n = 5$). (*J–L*) Results from cells treated with a combination of both ($n = 3$, $n = 6$).

REs to the sarcolemma (32–34). Similarly, here we report an endosomal pool of $Ca_V1.2$ channels that undergoes "on-demand" stimulated recycling upon activation of *βARs*, providing a functional reserve that drives ventricular inotropy during sympathetic stimulation.

Our work on live, AAV9-$Ca_V\beta_{2a}$–transduced AMVMs provides intriguing insights into $Ca_V1.2$ channel trafficking, and captures the complex dynamics of these channels. We find that these channels are often inserted into the sarcolemma as entire preformed clusters at nucleation sites. Sometimes, repetitive insertions were seen to occur at an individual site, conjuring an image of $Ca_V1.2$-carrying endosomes queued up along MTs, anchored at a sarcolemmal delivery hub. Furthermore, channel endocytosis often appeared to occur via removal of entire clusters, while in other cases, a slower, gradual removal of channels suggested ongoing removal of individual channels. Activation of *βARs* was observed to increase the probability of channel insertion. These scenarios were predicted in a recently published computer model designed to test the hypothesis that ion channel clustering occurs via a stochastic self-assembly process (35). Our data provide answers to the hypotheticals raised by that model, informing that model parameters with the experimental data acquired in this study would be an interesting sequel.

One well-characterized facet of cardiac $Ca_V1.2$ channel trafficking is their targeted anterograde-delivery to the t-tubule membrane along BIN1-anchored MTs via the biosynthetic delivery pathway (24). Reduced levels of BIN1 in cardiomyocytes isolated from failing human hearts are associated with impaired $Ca_V1.2$ channel delivery and slower onset calcium transients (7). Here, we find that $Ca_V1.2$ channel recycling also occurs along MTs. Three independent lines of evidence support this conclusion. First, MT disruption prevented ISO-stimulated mobilization of $Ca_V1.2$ from EE pools (Fig. 3*D*). Second, MT disruption significantly reduced stimulated channel insertions in AAV9-$Ca_V\beta_{2a}$-paGFP transduced AMVMs (Fig. 4*F* and Movie S2). Third, ISO-stimulated $Ca_V1.2$ superclustering was absent in nocodazole-treated AMVMs (Fig. 6 *B* and *E*). Our findings that basal $Ca_V1.2$ channel distribution and I_{Ca} amplitude were unaffected by 2-h nocodazole treatment suggests that channel lifetime in the membrane is longer than 2 h, so that channels delivered along intact MTs prior to depolymerization by the drug, still largely remained there (Fig. 6*B*). This agrees with previous measurements of PM $Ca_V1.2$ channel half-times of ∼3 h (9). However, despite negligible effects on basal channel expression and function, inhibition of MT polymerization significantly reduced ISO-stimulated responses, blunting I_{Ca} augmentation, and eliminating enhanced channel recycling and resultant superclustering. Reduced MT polymerization occurs in human heart failure where stabilized MTs form a dense network in cardiomyocytes (36, 37). The lack of polymerization and potentially enhanced MT catastrophe rates can result in traffic jams along MTs, leading to defective cargo delivery (36). Indeed, a previous study on live ventricular myocytes reported reduced delivery of $K_V4.2$ and $K_V4.3$ channels to the sarcolemma due to increased MT catastrophe rates upon addition of hydrogen peroxide or in the reactive oxygen species-rich postmyocardial infarction environment (38). Failing and aging myocytes display reduced $Ca_V1.2$ responsivity to ISO (39, 40), thus future studies should examine whether loss of

PHYSIOLOGY

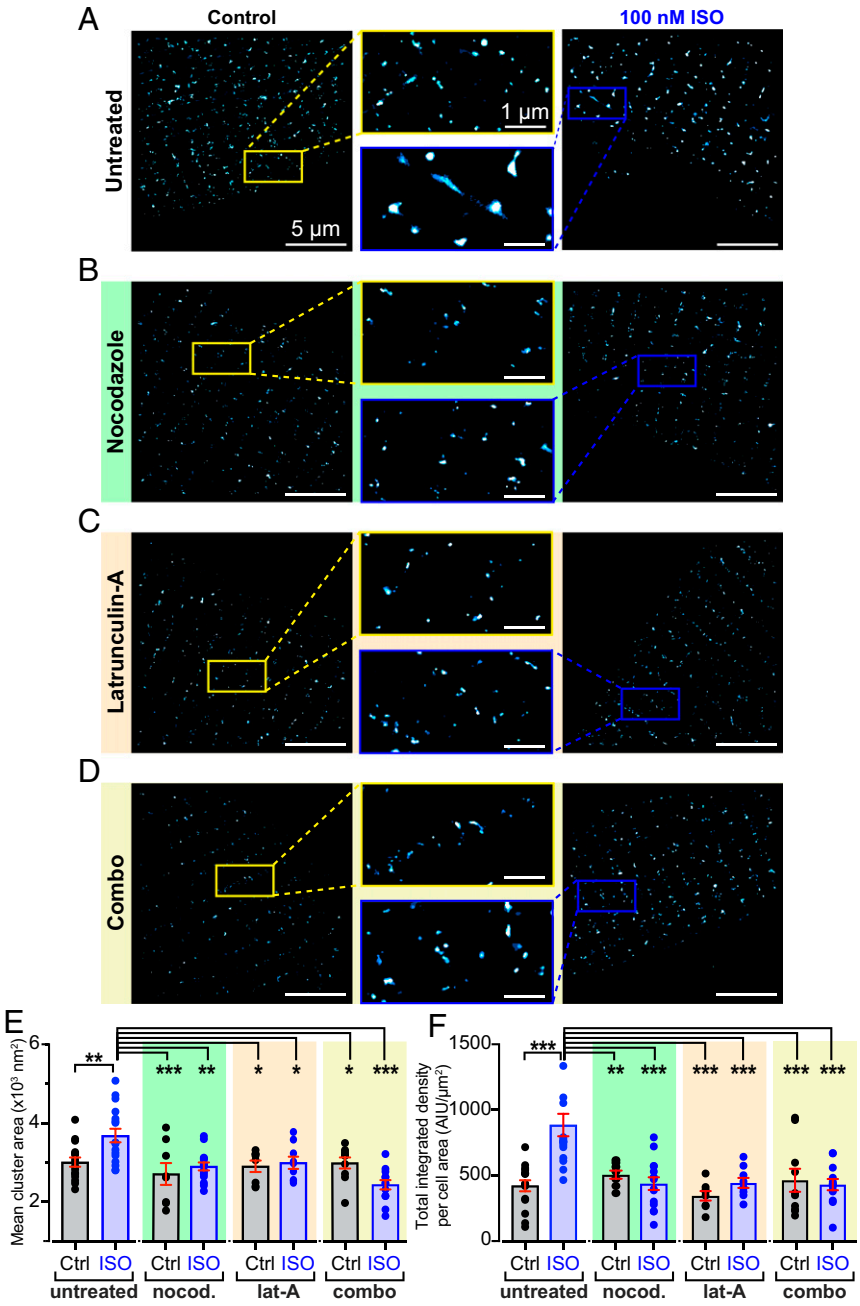

Fig. 6. βAR-stimulated $Ca_V1.2$ superclustering and enhanced sarcolemmal expression requires an intact MT cytoskeleton. Superresolution GSD localization maps of control (*Left*) and 100 nm ISO-stimulated (*Right*), fixed, AMVMs immunostained to examine $Ca_V1.2$ channel distribution under (*A*) untreated (control: $n = 4$, $n = 16$; ISO: $n = 4$, $n = 17$), (*B*) nocodazole-treated (control: $n = 3$, $n = 8$; ISO: ($n = 3$, $n = 15$), (C) lat-A–treated (control: $n = 3$, $n = 8$; ISO: ($n = 3$, $n = 9$), and (*D*) combo-treated (control: $n = 2$, $n = 10$; ISO: ($n = 3$, $n = 13$) conditions. Maps were pseudocolored "cyan hot" and received a one-pixel median filter for display purposes. Yellow (*control*) and blue (*ISO*) boxes indicate the location of the zoomed-in regions displayed in the center. (*E* and *F*) Aligned dot plots showing mean $Ca_V1.2$ channel cluster areas and normalized total integrated density in each condition. Two-way ANOVA. ***$P < 0.001$; **$P < 0.01$; *$P < 0.05$.

adrenergic responsivity of $Ca_V1.2$ in heart failure occurs due to impaired channel trafficking and recycling along MTs.

Actin polymerization has also been reported to be an important determinant of cardiac ion channel trafficking, notably of Cx43 (41). Although we failed to visualize cortical F-actin because of the vast amount of sarcomeric actin in AMVMs, we found that actin disruption with lat-A led to reduced: 1) ISO-stimulated mobilization of $Ca_V1.2$ from EEs (Fig. 3*H*), and 2) augmentation of $Ca_V1.2$ channel expression in the PM, as indicated by superresolution GSD imaging experiments (Fig. 6*C*) and live-cell TIRF experiments on AAV9-$Ca_V\beta_{2a}$-paGFP–transduced AMVMs (Fig. 4*E*). Furthermore, lat-A significantly blunted adrenergic regulation of the channels assessed with whole-cell patch clamp (Fig. 5 *G–I* and Table1). The degree of apparent channel insertions in response to ISO remained at a similar level to untreated cells, suggesting that MTs, not actin, play the dominant role in channel delivery to the sarcolemma (Fig. 4*F*). However, the pool of channels that was mobilized to the membrane in the presence of lat-A did not appear to belong to the EE pool, since colocalization between EEA1 and $Ca_V1.2$ channels was unchanged by ISO. In the Cx43 literature, it has been proposed that Cx43 cargo on its way to the sarcolemma from the Golgi along MTs, pauses at actin "rest stops" before being handed off to additional MTs to complete its journey to the membrane (41). It is possible that a similar rest stop system exists for $Ca_V1.2$ channel delivery in cardiomyocytes and that lat-A–mediated actin disruption and ISO-stimulation releases this pool, allowing them to traffic to the sarcolemma along MTs. This intriguing hypothesis remains to be proven.

On the basis of our functional patch-clamp data, it is tempting to speculate that *βAR*-mediated regulation of $Ca_V1.2$ is heavily dependent on this stimulated channel recycling pathway; however,

ISO-stimulation is also known to induce endocytosis and subsequent fast, actin-dependent recycling and resensitization of the receptors themselves (42, 43). It is therefore possible that the lack of functional response is simply because of a lack of sarcolemmal *βAR* expression, as internalized receptors cannot recycle back to the membrane (44). To investigate this possibility, we bypassed the receptors and stimulated adenylyl cyclase directly with forskolin (*SI Appendix*, Fig. S8). Forskolin (1 μM) produced a similar increase in sarcolemmal $Ca_V\beta_{2a}$-paGFP expression (21.60 ± 3.72%) to that observed with 100 nM ISO (27.95 ± 4.31%). Treatment of AMVMs with cytoskeletal disruptors reduced the response (*SI Appendix*, Fig. S8 *B–E*). Further examination of βAR-stimulation of cAMP production using an PM-targeted FRET-based cAMP sensor (lynICUE3) (45) revealed no significant alteration with cytoskeletal disruptors (*SI Appendix*, Fig. S9). These data suggest that the effects of cytoskeletal disruptors on channel responses to adrenergic stimulation are unlikely to be caused by less robust βAR-signaling and cannot explain the observed abolition of *βAR*-regulation of I_{Ca} (Fig. 5). It is also possible that the morphology and composition of the PM could be altered by cytoskeletal disruptors. While we cannot completely exclude this, superresolution images did not expose any overt alteration in t-tubule regularity, and capacitance measurements (*SI Appendix*, Fig. S5*F*) made during whole-cell recordings revealed no significant change in membrane area with any of the treatments. Overall, these results suggest that agonist-stimulated recycling of $Ca_V1.2$ is in fact a critical component of *βAR*-regulation of these channels.

The critical PKA phosphorylation site on the cardiac $Ca_V1.2$ channel complex was recently reported to be located on Rad, a member of the Rad/Rem/Rem2/Gem/Kir (RGK) family of monomeric GTP-binding proteins that interacts with the channel via the β-subunit (4). In a disinhibition process, Rad phosphorylation is proposed to dissociate from the channel complex, releasing its inhibitory hold on the channel and unveiling the hallmark larger I_{Ca} during *βAR*-activation. A Rad-mediated $Ca_V1.2$ disinhibition hypothesis was also proposed several years earlier by Jonathan Satin's group (46) when they reported that Rad knockout mice are refractory to adrenergic receptor stimulation.

So how does our *βAR*-stimulated recycling of $Ca_V1.2$ fit into this appealing model? We do not believe the two models are mutually exclusive but instead hypothesize that Rad inhibits $Ca_V1.2$ channel function by limiting its expression at the sarcolemma, an effect that is relieved when Rad is phosphorylated by PKA. Indeed, in addition to the ability of Rad to suppress channel activity by interfering with channel P_o, it has long been reported that RGK-proteins, including Rad, also reduce I_{Ca} by limiting $Ca_V1.2$ expression at the sarcolemma (47, 48). Our results in transduced AMVMs and tsA cells illustrate that ISO-stimulates enhanced transport of channels to the PM. We speculate that this transport could occur when Rad is phosphorylated and dislodges from $Ca_V\beta$, releasing the channel complex and allowing more to traffic to the surface in a Rab4a- and Rab11a-dependent process. Phosphorylation of Rad may be the "upstream step" that has to occur before this recycling process is initiated, explaining why overexpression of CA-Rab4a does not raise the initial expression of $Ca_V1.2$ in the membrane in and of itself, but rather Rad phosphorylation must occur first. The resultant increase in the number of channels in the PM would be predicted to up-regulate I_{Ca}, since $I_{Ca} = N \times i_{Ca} \times P_o$, where (N) is the number of channels, (P_o) is their open probability, and (i_{Ca}) is their single-channel current.

We have previously reported that *βAR*-stimulation with ISO facilitates cooperative interactions between adjacent channels, amplifying Ca^{2+} influx (17). In addition, there is evidence that gating of cooperatively interacting channels is driven by the highest activity channels in the cluster (49). The relationship between ISO-stimulated channel insertions and current density augmentation thus may not be linear, since stimulated insertion of a small number of phosphorylated, Rad-dissociated, high P_o channels could have a disproportionately large effect on I_{Ca}, driving associated channels to a higher P_o, and generating the signature increase in I_{Ca} and P_o of PKA-regulation of $Ca_V1.2$.

How PKA is anchored next to Rad on endosomes is another matter but may depend on the A-kinase–anchoring protein D-AKAP2, which has been reported to regulate recycling of transferrin receptors via interactions with Rab4 and Rab11 (50). In line with that prediction, a human functional polymorphism in D-AKAP2 (I646V) is associated with reduced heart rate variability, indicative of a heart that cannot respond well to stressors (51). D-AKAP2 itself can be phosphorylated by PKA at residue 554 (50), and this may influence its localization. We briefly tested the hypothesis that ISO-stimulation of *βARs* would promote enhanced colocalization between D-AKAP2 and $Rab11^+$ endosomes finding an enhanced association (*SI Appendix*, Fig. S10). While this is admittedly a correlative result, resolving these mechanistic details will make for an interesting future project.

Overall, our data indicate that cardiomyocytes have an endosomal reservoir of $Ca_V1.2$ channels that is rapidly mobilized to the t-tubule sarcolemma in response to *βAR*-stimulation, and that this stimulated insertion is fundamentally required for *βAR*-regulation of these channels.

Materials and Methods

Detailed methods can be found in *SI Appendix*. Briefly, AMVMs were enzymatically isolated using standard Langendorff technique as described previously (17). Fixed, immunostained AMVMs were imaged on a Zeiss Airyscan confocal microscope or a Leica 3D-GSD-SR microscope to assess the distribution of $Ca_V1.2$ channels and various endosome populations. Live-cell TIRF imaging experiments of AAV9-$Ca_V\beta_{2a}$-paGFP–transduced AMVMs or transiently transfected tsA-201 cells were performed on an Olympus IX-83 inverted microscope with a Cell-TIRF MITICO module. Live-cell 4D-imaging of transduced AMVMs was performed at 37 °C on an Andor W-1 Spinning Disk confocal microscope. Rab mutant plasmids used for transient transfection of tsA-201 cells were gifts from Nipavan Chiamvimonvat, University of California, Davis, CA, and Jose A. Esteban, Centro de Biología Molecular 'Severo Ochoa', Consejo Superior de Investigaciones Científicas-Universidad Autónoma, Madrid, Spain.

Data Availability. All study data are included in the article and supporting information.

ACKNOWLEDGMENTS. We thank Dr. Luis Fernando Santana for the use of his Ground-State Depletion microscope, and for reading and commenting on this manuscript; and Dr. Yang K. Xiang for the use of his FRET system. This work was supported by NIH National Institute on Aging Grant R01AG063796 and American Heart Association Grant 15SDG25560035 (to R.E.D.); National Institute of General Medical Sciences Grant R01GM127513 (to E.J.D.); and National Heart, Lung, and Blood Institute Grants R01HL121059 and R01HL149127 (to M.F.N.). T.L.V. and H.C.S. were supported by a National Institute of General Medical Sciences-funded Pharmacology Training Program (T32GM099608).

1. H. Reuter, H. Scholz, The regulation of the calcium conductance of cardiac muscle by adrenaline. *J. Physiol.* **264**, 49–62 (1977).
2. D. T. Yue, S. Herzig, E. Marban, Beta-adrenergic stimulation of calcium channels occurs by potentiation of high-activity gating modes. *Proc. Natl. Acad. Sci. U.S.A.* **87**, 753–757 (1990).
3. N. Sperelakis, J. A. Schneider, A metabolic control mechanism for calcium ion influx that may protect the ventricular myocardial cell. *Am. J. Cardiol.* **37**, 1079–1085 (1976).
4. G. Liu *et al.*, Mechanism of adrenergic $Ca_V1.2$ stimulation revealed by proximity proteomics. *Nature* **577**, 695–700 (2020).
5. J. He *et al.*, Reduction in density of transverse tubules and L-type $Ca^{(2+)}$ channels in canine tachycardia-induced heart failure. *Cardiovasc. Res.* **49**, 298–307 (2001).
6. I. R. Josephson, A. Guia, M. D. Stern, E. G. Lakatta, Alterations in properties of L-type Ca channels in aging rat heart. *J. Mol. Cell. Cardiol.* **34**, 297–308 (2002).
7. T. T. Hong *et al.*, BIN1 is reduced and Cav1.2 trafficking is impaired in human failing cardiomyocytes. *Heart Rhythm* **9**, 812–820 (2012).
8. I. Pranke, A. Golec, A. Hinzpeter, A. Edelman, I. Sermet-Gaudelus, Emerging therapeutic approaches for cystic fibrosis. From gene editing to personalized medicine. *Front. Pharmacol.* **10**, 121 (2019).

9. A. J. Chien *et al*., Roles of a membrane-localized beta subunit in the formation and targeting of functional L-type Ca^{2+} channels. *J. Biol. Chem.* **270**, 30036–30044 (1995).
10. R. Conrad *et al*., Rapid turnover of the cardiac L-type $Ca_V1.2$ channel by endocytic recycling regulates its cell surface availability. *iScience* **7**, 1–15 (2018).
11. P. Buda *et al*., Eukaryotic translation initiation factor 3 subunit e controls intracellular calcium homeostasis by regulation of $ca_v1.2$ surface expression. *PloS One* **8**, e64462 (2013).
12. H. Stenmark, Rab GTPases as coordinators of vesicle traffic. *Nat. Rev. Mol. Cell Biol.* **10**, 513–525 (2009).
13. F. R. Maxfield, T. E. McGraw, Endocytic recycling. *Nat. Rev. Mol. Cell Biol.* **5**, 121–132 (2004).
14. E. M. Green, C. F. Barrett, G. Bultynck, S. M. Shamah, R. E. Dolmetsch, The tumor suppressor eIF3e mediates calcium-dependent internalization of the L-type calcium channel CaV1.2. *Neuron* **55**, 615–632 (2007).
15. J. M. Best *et al*., Small GTPase Rab11b regulates degradation of surface membrane L-type Cav1.2 channels. *Am. J. Physiol. Cell Physiol.* **300**, C1023–C1033 (2011).
16. D. Ghosh *et al*., Dynamic L-type $Ca_V1.2$ channel trafficking facilitates $Ca_V1.2$ clustering and cooperative gating. *Biochim. Biophys. Acta Mol. Cell Res.* **1865**, 1341–1355 (2018).
17. D. W. Ito *et al*., β-Adrenergic-mediated dynamic augmentation of sarcolemmal Ca_V 1.2 clustering and co-operativity in ventricular myocytes. *J. Physiol.* **597**, 2139–2162 (2019).
18. B. K. Atwood, J. Lopez, J. Wager-Miller, K. Mackie, A. Straiker, Expression of G protein-coupled receptors and related proteins in HEK293, AtT20, BV2, and N18 cell lines as revealed by microarray analysis. *BMC Genomics* **12**, 14 (2011).
19. M. Cormont *et al*., Potential role of Rab4 in the regulation of subcellular localization of Glut4 in adipocytes. *Mol. Cell Biol.* **16**, 6879–6886 (1996).
20. S. C. Calaghan, J. Y. Le Guennec, E. White, Cytoskeletal modulation of electrical and mechanical activity in cardiac myocytes. *Prog. Biophys. Mol. Biol.* **84**, 29–59 (2004).
21. S. X. Takahashi, S. Mittman, H. M. Colecraft, Distinctive modulatory effects of five human auxiliary β2 subunit splice variants on L-type calcium channel gating. *Biophys. J.* **84**, 3007–3021 (2003).
22. J. Miriyala, T. Nguyen, D. T. Yue, H. M. Colecraft, Role of CaVbeta subunits, and lack of functional reserve, in protein kinase A modulation of cardiac CaV1.2 channels. *Circ. Res.* **102**, e54–e64 (2008).
23. B. D. Grant, J. G. Donaldson, Pathways and mechanisms of endocytic recycling. *Nat. Rev. Mol. Cell Biol.* **10**, 597–608 (2009).
24. T. T. Hong *et al*., BIN1 localizes the L-type calcium channel to cardiac T-tubules. *PLoS Biol.* **8**, e1000312 (2010).
25. D. D. Hall *et al*., Competition between α-actinin and Ca^{2+}-calmodulin controls surface retention of the L-type Ca^{2+} channel Ca(V)1.2. *Neuron* **78**, 483–497 (2013).
26. P. Y. Tseng *et al*., α-Actinin promotes surface localization and current density of the Ca^{2+} channel $Ca_V1.2$ by binding to the IQ region of the α1 subunit. *Biochemistry* **56**, 3669–3681 (2017).
27. A. Chase, J. Colyer, C. H. Orchard, Localised Ca channel phosphorylation modulates the distribution of L-type Ca current in cardiac myocytes. *J. Mol. Cell. Cardiol.* **49**, 121–131 (2010).
28. R. C. Balijepalli, J. D. Foell, D. D. Hall, J. W. Hell, T. J. Kamp, Localization of cardiac L-type $Ca^{(2+)}$ channels to a caveolar macromolecular signaling complex is required for $\beta(_2)$-adrenergic regulation. *Proc. Natl. Acad. Sci. U.S.A.* **103**, 7500–7505 (2006).
29. G. H. Diering, R. L. Huganir, The AMPA receptor code of synaptic plasticity. *Neuron* **100**, 314–329 (2018).
30. P. I. Nedvetsky *et al*., A Role of myosin Vb and Rab11-FIP2 in the aquaporin-2 shuttle. *Traffic* **8**, 110–123 (2007).
31. K. Fushimi, S. Sasaki, F. Marumo, Phosphorylation of serine 256 is required for cAMP-dependent regulatory exocytosis of the aquaporin-2 water channel. *J. Biol. Chem.* **272**, 14800–14804 (1997).
32. L. Bao, K. Hadjiolova, W. A. Coetzee, M. J. Rindler, Endosomal KATP channels as a reservoir after myocardial ischemia: A role for SUR2 subunits. *Am. J. Physiol. Heart Circ. Physiol.* **300**, H262–H270 (2011).
33. Y. Wang *et al*., $[Ca^{2+}]_i$ elevation and oxidative stress induce KCNQ1 protein translocation from the cytosol to the cell surface and increase slow delayed rectifier (IKs) in cardiac myocytes. *J. Biol. Chem.* **288**, 35358–35371 (2013).
34. G. Seebohm *et al*., Regulation of endocytic recycling of KCNQ1/KCNE1 potassium channels. *Circ. Res.* **100**, 686–692 (2007).
35. D. Sato *et al*., A stochastic model of ion channel cluster formation in the plasma membrane. *J. Gen. Physiol.* **151**, 1116–1134 (2019).
36. M. A. Caporizzo, C. Y. Chen, B. L. Prosser, Cardiac microtubules in health and heart disease. *Exp. Biol. Med.* **244**, 1255–1272 (2019).
37. C. Y. Chen *et al*., Suppression of detyrosinated microtubules improves cardiomyocyte function in human heart failure. *Nat. Med.* **24**, 1225–1233 (2018).
38. B. M. Drum *et al*., Oxidative stress decreases microtubule growth and stability in ventricular myocytes. *J. Mol. Cell. Cardiol.* **93**, 32–43 (2016).
39. H. Ouadid, B. Albat, J. Nargeot, Calcium currents in diseased human cardiac cells. *J. Cardiovasc. Pharmacol.* **25**, 282–291 (1995).
40. J. B. Strait, E. G. Lakatta, Aging-associated Cardiovascular changes and their relationship to heart failure. *Heart Failure Clinics* **8**, 143 (2012).
41. J. W. Smyth *et al*., Actin cytoskeleton rest stops regulate anterograde traffic of connexin 43 vesicles to the plasma membrane. *Circ. Res.* **110**, 978–989 (2012).
42. A. C. Hanyaloglu, M. von Zastrow, Regulation of GPCRs by endocytic membrane trafficking and its potential implications. *Annu. Rev. Pharmacol. Toxicol.* **48**, 537–568 (2008).
43. G. A. Yudowski, M. A. Puthenveedu, A. G. Henry, M. von Zastrow, Cargo-mediated regulation of a rapid Rab4-dependent recycling pathway. *Mol. Biol. Cell* **20**, 2774–2784 (2009).
44. E. E. Millman *et al*., Rapid recycling of beta-adrenergic receptors is dependent on the actin cytoskeleton and myosin Vb. *Traffic* **9**, 1958–1971 (2008).
45. L. M. DiPilato, X. Cheng, J. Zhang, Fluorescent indicators of cAMP and Epac activation reveal differential dynamics of cAMP signaling within discrete subcellular compartments. *Proc. Natl. Acad. Sci. U.S.A.* **101**, 16513–16518 (2004).
46. J. R. Manning *et al*., Rad GTPase deletion increases L-type calcium channel current leading to increased cardiac contraction. *J. Am. Heart Assoc.* **2**, e000459 (2013).
47. P. Béguin *et al*., Nuclear sequestration of beta-subunits by Rad and Rem is controlled by 14-3-3 and calmodulin and reveals a novel mechanism for Ca^{2+} channel regulation. *J. Mol. Biol.* **355**, 34–46 (2006).
48. P. Béguin *et al*., Regulation of Ca^{2+} channel expression at the cell surface by the small G-protein kir/Gem. *Nature* **411**, 701–706 (2001).
49. R. E. Dixon, C. Yuan, E. P. Cheng, M. F. Navedo, L. F. Santana, Ca^{2+} signaling amplification by oligomerization of L-type $Ca_v1.2$ channels. *Proc. Natl. Acad. Sci. U.S.A.* **109**, 1749–1754 (2012).
50. C. T. Eggers, J. C. Schafer, J. R. Goldenring, S. S. Taylor, D-AKAP2 interacts with Rab4 and Rab11 through its RGS domains and regulates transferrin receptor recycling. *J. Biol. Chem.* **284**, 32869–32880 (2009).
51. S. A. Neumann *et al*., AKAP10 (I646V) functional polymorphism predicts heart rate and heart rate variability in apparently healthy, middle-aged European-Americans. *Psychophysiology* **46**, 466–472 (2009).